Section I: Basic and Applied Research

To Journal of Phase Equilibria and Diffusion Phase Relationship of the BaO-ZrO$_2$-YO$_{1.5}$ System at 1500 and 1600 °C

Susumu Imashuku, Tetsuya Uda, Yoshitaro Nose, and Yasuhiro Awakura

(Submitted October 16, 2009; in revised form March 17, 2010)

Phase relationship of a BaO-ZrO$_2$-YO$_{1.5}$ system at 1500 and 1600 °C was examined in order to determine whether a phase separation at the composition of 15% yttrium-doped barium zirconate exists. According to a pseudoternary phase diagram of the BaO-ZrO$_2$-YO$_{1.5}$ system established by this work, the solubility of yttria into cubic barium zirconate at 1600 °C is 0.25 in a mole fraction of yttria ($X_{YO_{1.5}}$). Thus, we confirmed that there is no phase separation at the composition of 15% yttrium-doped barium zirconate at 1600 °C. On the other hand, at 1500 °C, there might be a phase separation at the composition of 15% yttrium-doped barium zirconate into yttrium-doped barium zirconate where quite small amount of yttrium is doped and a new phase whose composition is close to reported BZ(II) phase.

1. Introduction

The crystallographic structure of barium zirconate (BaZrO$_3$) belongs to the perovskite-type, and trivalent cation (M(III))-doped barium zirconate has been reported to be a proton conductive oxide.[1,2] It has great potential for applications, e.g., electrolytes for fuel cells, hydrogen separation membrane, and hydrogen sensors. Yttrium-doped barium zirconate is known to have the lowest protonic resistance of grain interior among trivalent cation-doped barium zirconate and this property attracts many researchers.[3-22] In the previous works, we investigated a sintering mechanism of 15% yttrium-doped barium zirconate (BaZr$_{0.85}$Y$_{0.15}$O$_{3-\delta}$) at 1600 °C based on the idea of two-phase separation of yttrium poor barium zirconate and yttrium rich barium zirconate phase in the sample by conventional solid state reaction.[19,20] A phase separation at 1600 °C was reported by Kojima et al.[23] However, the points we discussed are that there is no phase separation in equilibrium at 1600 °C, but traces of the phase separation at synthesizing temperature, 1300 °C, might remain even at 1600 °C. This residual phase with different composition makes the grain growth rate slow because a long-distance diffusion of cations is needed for the grain growth. Based on the proposed mechanism, we succeed in sintering well-grain-grown 15% yttrium-doped barium zirconate with a

Susumu Imashuku, Tetsuya Uda, Yoshitaro Nose, and Yasuhiro Awakura, Department of Materials Science and Engineering, Kyoto University, Yoshida-Honmachi, Sakyo, Kyoto 606-8501, Japan. Contact e-mail: materials_process@aqua.mtl.kyoto-u.ac.jp.

powder obtained by a nitrate freeze-drying method and synthesis at 500 °C which is finer and more homogeneous than that by solid state reaction route.[22]

In this study, we try to provide the evidence of the phase separation by investigating phase relationships of a BaO-ZrO$_2$-YO$_{1.5}$ system at synthesizing temperature, 1300 °C, and sintering temperature, 1600 °C. However, it was very difficult to obtain phase equilibration at the synthesizing temperature, at 1300 °C, due to a kinetic reason,[20] this study has investigated the phase relationship of the BaO-ZrO$_2$-YO$_{1.5}$ system at 1500 °C, instead of 1300 and 1600 °C.

2. Experimental

2.1 Material Preparation

Powders obtained by a nitrate freeze-drying method were used to achieve equilibrium in short time. The reagents were barium nitrate (Ba(NO$_3$)$_2$: 99.9%, Wako), zirconyl nitrate dihydrate (ZrO(NO$_3$)$_2 \cdot 2$H$_2$O: 97.0%, Wako), and yttrium nitrate n-hydrate (Y(NO$_3$)$_3 \cdot n$H$_2$O: 99.9%, Wako). Zirconyl nitrate dihydrate was dissolved in 0.1 M nitric acid (HNO$_3$) and then the solution was filtered to remove a small amount of zirconia (ZrO$_2$) in the solution. Yttrium nitrate n-hydrate was dissolved in 0.1 M nitric acid. The concentrations of the two solutions were measured by inductive coupled plasma-atomic emission spectroscopy (ICP-AES) (Seiko Instruments Inc., SPS4000). The zirconyl nitrate solution contained 2.07 mass% of hafnium (Hf) as an impurity. The chemical properties of hafnium are quite similar to those of zirconium. Thus, hafnium is expected to occupy the zirconium site and to behave very much like zirconium. In addition, 2.07 mass% of hafnia (HfO$_2$) corresponds to only 1.08 mol.% of hafnia in a ZrO$_2$-HfO$_2$ system. Such a small percentage might have a very small effect on the phase relationship. Thus, the effect of hafnia was neglected on the

results. Then, the two solutions of zirconyl nitrate and yttrium nitrate were mixed with barium nitrate powder. The composition of the mixed solution was confirmed again by ICP-AES, and the barium concentration of the mixed solution was about 0.08 M. About 250 mL of the mixed solution was atomized using an ultrasonic spray nozzle (Sonotek, 06-5108) and rapidly frozen by leading the aerosol to fall into stirred liquid nitrogen. The frozen solution was vacuum-dried in a freeze dryer (DRC-1100 and FDU-2100, EYEA) under the controlled pressure and temperature (5 Pa, -40 °C). After that, the temperature was gradually heated to 25 °C in the same chamber. When the powder was completely dried at 25 °C, the vacuum chamber was backfilled with air. This procedure took about 4 days to obtain the dried powder. The powder was heated at 500 °C for 10 h in vacuum and ball-milled for 10 h. The powder was pressed into a pellet at 392 MPa. Subsequently, the pellet was moved to a furnace already heated at 1600 °C and then kept at the temperature for 24 h in air. The same procedure was conducted at 1500 °C, but the holding time was 100 h. The heated samples were quenched to room temperature. At elevated temperatures, barium oxide (BaO) has a significantly high vapor pressure (ca, 8×10^{-5} atm at 1600 °C[24]) and the evaporation of barium oxide from the sample must be considered. Because this evaporation may lead to a significant deviation from the nominal composition during the heat-treatment, sacrifice powders which consist of 90 mass% of the same composition as the pellet and 10 mass% of barium carbonate (BaCO$_3$: 99.9%, Wako) were used to minimize the composition changes due to the vaporization of barium oxide from the samples except for the experiments with samples containing $X_{BaO} = 0.30$ as a mole fraction. The sacrifice powders were synthesized by a conventional solid state reaction.[10,18-20] The heat-treatment sample temperatures were checked using a thermal history

sensor (Referthomo type H, AS ONE). The temperature deviation in the experiments was within 1600 ± 10 and 1500 ± 5 °C.

2.2 Chemical Analysis and Phase Identification

The nominal compositions and compositions of quenched samples are listed in Table 1. The nominal compositions of samples were compositions of freeze-dried powders before heat-treatment which are measured by ICP-AES. The compositions of quenched samples were also measured by ICP-AES except for samples A, B, C, and N where zirconia precipitated. Figure 1 shows the nominal compositions (samples A to C, N) and compositions of
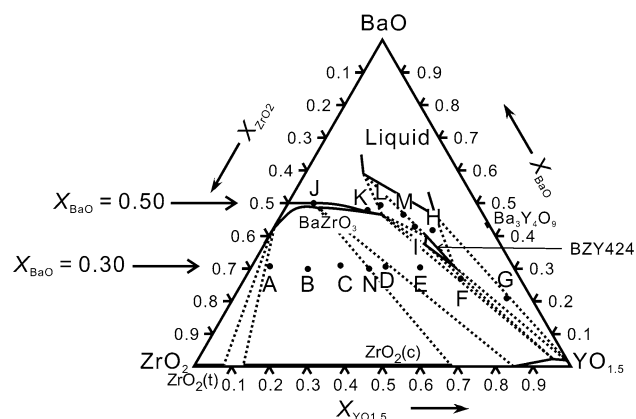

Fig. 1 Nominal compositions (samples A to C) and compositions of quenched samples (samples D to M) used in this study. Abbreviations of sample names are referred to Table 1. *Dotted lines* are proposed phase boundaries at 1600 °C

Table 1 Nominal compositions, compositions of quenched samples and phases identified by x-ray diffraction in samples heat-treated at 1600 °C for 24 h

Sample	Nominal composition			Composition after quench			Identified phase by XRD after heat-treatment at 1600 °C			
	X_{BaO}	X_{ZrO_2}	$X_{YO_{1.5}}$	X_{BaO}	X_{ZrO_2}	$X_{YO_{1.5}}$	BaZrO$_3$	ZrO$_2$ (cubic)	Y$_2$O$_3$	Unknown
A	0.303	0.638	0.052	-	-	-	○	○	×	×
B	0.299	0.540	0.156	-	-	-	○	○	×	×
C	0.304	0.444	0.247	-	-	-	○	?	?	×
D	0.305	0.340	0.351	0.298	0.335	0.364	○	?	?	×
E	0.313	0.250	0.434	0.301	0.250	0.446	○	×	○	×
F	0.306	0.151	0.542	0.269	0.146	0.583	○	×	○	×
G	0.301	0.064	0.635	0.209	0.060	0.731	○	×	○	○
H	0.399	0.177	0.423	0.411	0.166	0.421	?	×	○	○
I	0.408	0.206	0.384	0.421	0.196	0.381	?	×	○	○
J	0.499	0.422	0.075	0.502	0.419	0.075	○	×	×	×
K	0.497	0.301	0.198	0.490	0.300	0.207	○	×	×	×
L	0.490	0.260	0.247	0.493	0.251	0.253	○	×	×	○
M	0.496	0.200	0.302	0.472	0.206	0.320	○	×	×	○
N	0.296	0.299	0.402	-	-	-	-	-	-	-

○: detected, ×: undetected, ?: cannot be judged only by XRD, and -: not investigated

quenched samples (samples D to M) on a pseudoternary phase diagram of the BaO-ZrO$_2$-YO$_{1.5}$ system.

The compositions of each grain in quenched samples were point-analyzed by energy dispersive x-ray microanalysis (EDX) (JEOL, JED-2300) equipped with field emission-scanning electron microscope (FE-SEM) (JEOL, JSM-6500F) and calibrated based on the assumption that the average compositions of samples area-analyzed by EDX are equal to the nominal compositions (samples A to C and N) or compositions of quenched samples (samples D to M) by ICP-AES.

The phases in quenched samples were identified by x-ray diffraction analysis (XRD, PANalytical, X'part-ProMPD, Cu-Kα) and the results are listed in Table 1.

3. Results and Discussion

We established the pseudoternary phase diagram of the BaO-ZrO$_2$-YO$_{1.5}$ system at 1600 °C as shown in Fig. 2. To establish this phase diagram, we combined information of experimental pseudobinary phase diagrams of the BaO-ZrO$_2$ system,[25] the BaO-YO$_{1.5}$ system[26-29] and the ZrO$_2$-YO$_{1.5}$ system[30] in air. Several phase diagrams of the BaO-YO$_{1.5}$ system were available, the phase relationship of the system at 1600 °C coincides with each other.[26-29] On the other hand, many proposed experimental phase diagrams of the ZrO$_2$-YO$_{1.5}$ system were reported.[30-36] There are a few contradiction among the reports; the solubility of yttria into tetragonal and cubic zirconia phase, and the solubility of zirconia into yttria at 1600 °C.[33,34] As for the solubility of yttria into zirconia phases (tetragonal and cubic phases), we adopted the data by Srivastava et al.[30] because their data match well with many other measurements and our

results at 1600 °C. Meanwhile, as for the solubility of zirconia into yttria, we adopted our data. We provide the detailed results and discussion for the established phase diagram as follows.

3.1 Analysis of XRD and EDX on X_{BaO} = 0.30 at 1600 °C

First, samples on the composition line of X_{BaO} = 0.30 (samples A to G) were prepared and heat-treated at 1600 °C for 24 h. XRD patterns of the samples after heat-treatment are shown in Fig. 3(a) and (b), and the identified phases are summarized in Table 1. The compositions of each grain are shown on pseudoternary phase diagrams of BaO-ZrO$_2$-YO$_{1.5}$ system in Fig. 4(a) and (b). When grains in samples are very fine, the composition point-analyzed by EDX might be an average value of two or more grains with different compositions because the spot size of the electron beam in FE-SEM is wider than the size of grains and the penetrated beam spreads into a few grains. Consequently, if we analyzed a mixture of two grains with different compositions, the analyzed compositions would be on lines connecting composition points of the different grains on the pseudoternary phase diagram of the BaO-ZrO$_2$-YO$_{1.5}$ system. Thus, we adopted the compositions at the end of the connected lines as compositions of each grain. Then, we confirmed five types of grains (cubic barium zirconate phase, BZY424 phase, cubic zirconia phase, yttria phase, and liquid phase) by combining the result of XRD in this study and the compositions summarized in Table 2. The details are described in the next paragraph.

When the mole fraction of yttria was 0.052 ($X_{\mathrm{YO}_{1.5}}$ = 0.052 (sample A)) and 0.156 ($X_{\mathrm{YO}_{1.5}}$ = 0.156 (sample B)), cubic barium zirconate phase (BaZrO$_3$(ss)) and cubic zirconia phase were identified by XRD analysis. As seen in Fig. 3(a), the peak positions of the cubic zirconia phase in
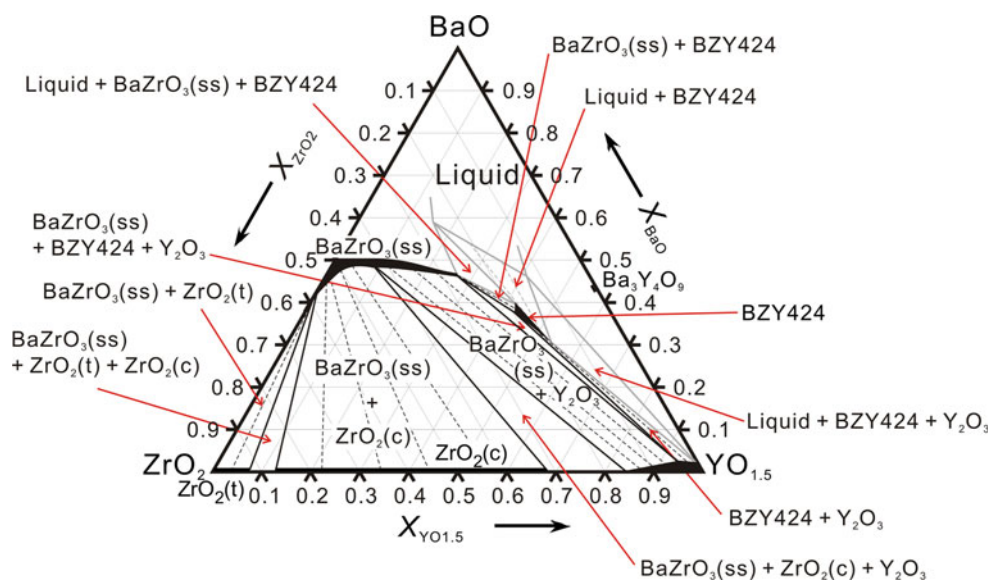

Fig. 2 Established pseudoternary phase diagram of the BaO-ZrO$_2$-YO$_{1.5}$ system at 1600 °C. ZrO$_2$(t) and ZrO$_2$(c) denote tetragonal zirconia and cubic zirconia, respectively
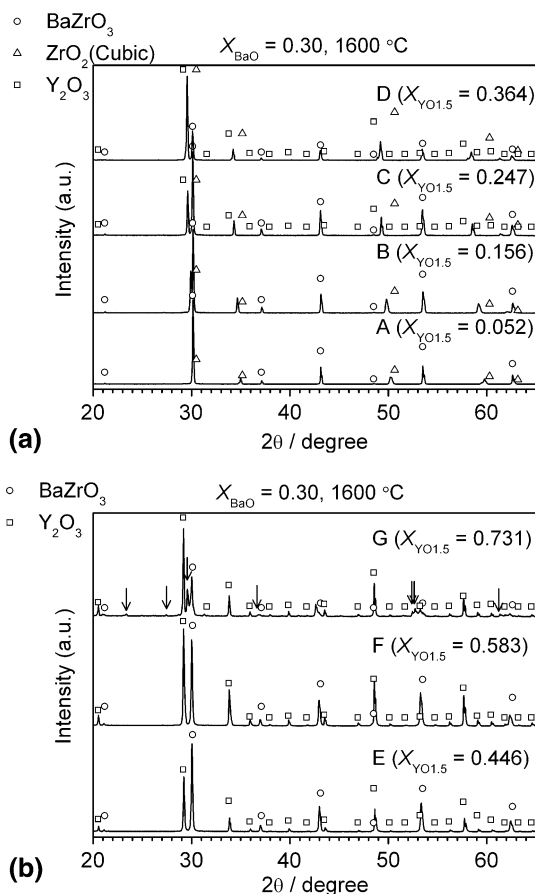
(a)

(b)

Fig. 3 XRD patterns of samples at $X_{BaO} = 0.30$ after heat-treatment at 1600 °C for 24 h ((a) samples A to D, (b) samples E to G). Each symbol indicates diffraction patterns of ○ (BaZrO₃, JCPDS No. 00-006-0399), △ (ZrO₂, JCPDS No. 00-027-0997), and □ (Y₂O₃, JCPDS No. 00-043-1036). Unknown peaks are indicated by *arrows*, ↓

sample B shifted to lower angles than those of the cubic zirconia phase in JCPDS card [No. 00-027-0997, lattice parameter, $a = 0.50900$ nm], which is due to dissolution of yttria into the cubic zirconia phase as reported by Pascual and Duran.[35] The results measured by EDX also support that by XRD. When $X_{YO_{1.5}} = 0.247$ (sample C) and 0.364 (sample D), cubic barium zirconate phase (BaZrO₃(ss)) was identified by XRD analysis, but we could not determine whether peak patterns other than cubic barium zirconate phase (BaZrO₃(ss)) belong to yttria phase or cubic zirconia phase. But, a grain in sample C, whose composition is $X_{BaO} = 0$, $X_{ZrO_2} = 0.42$, and $X_{YO_{1.5}} = 0.58$, was detected by EDX analysis, which is within the solubility of yttria into zirconia at 1600 °C; $X_{YO_{1.5}} = 0.69$.[30] Thus, we considered that sample C consists of cubic barium zirconate phase (BaZrO₃(ss)) and cubic zirconia phase. On the other hand, the composition of the grain in sample D was $X_{BaO} = 0.01$, $X_{ZrO_2} = 0.16$, and $X_{YO_{1.5}} = 0.83$ by EDX analysis. Combining the compositions of the grain and barium zirconate by EDX and total composition of sample D by ICP-AES, sample D should be in three-phase region of cubic barium

zirconate phase, cubic zirconia phase, and yttria phase. However, we could not detect the grains of cubic zirconia phase by EDX analysis. This is probably due to the small existence ratio of cubic zirconia phase. If we can assume that sample D is in the three-phase region, the solubility of zirconia into yttria phase is $X_{ZrO_2} = 0.16$. This solubility is a little larger than the reported solubility ($X_{ZrO_2} = 0.10$,[31] 0.11[30]) and further investigation is needed. When $X_{YO_{1.5}} = 0.446$ (sample E) and 0.583 (sample F), cubic barium zirconate phase (BaZrO₃(ss)) and yttria phase were identified by XRD analysis (Fig. 3b). However, there were two kinds of grains which consist of barium, yttrium, and zirconium in sample F by EDX analysis. One is cubic barium zirconate phase (BaZrO₃(ss)) from the composition, and the other is considered to be a new phase. But, we could not distinguish between these two phases by XRD. When $X_{YO_{1.5}} = 0.731$ (sample G), cubic barium zirconate phase (BaZrO₃(ss)), yttria phase and an unknown phase shown by arrows were identified by XRD (see Fig. 3b). From the result of EDX analysis in Table 2, one of the detected phases in sample G ($X_{BaO} = 0.31$, $X_{ZrO_2} = 0.16$, and $X_{YO_{1.5}} = 0.53$) corresponds to the new phase in sample F. We call the new phase as BZY424 phase in this paper. Additionally, another kind of grain, whose composition was $X_{BaO} = 0.47$, $X_{ZrO_2} = 0.12$, and $X_{YO_{1.5}} = 0.41$, was observed by EDX analysis in sample G. Tabular grains were observed by SEM as shown in Fig. 5. The existence of liquid phase at BaO-rich region at 1600 °C was reported by Kojima et al.[23] Thus, the grain with $X_{BaO} = 0.47$, $X_{ZrO_2} = 0.12$, and $X_{YO_{1.5}} = 0.41$ is considered to be a solidified liquid phase. It is also noted that such large solidus grains have never been observed in the system after sintering at 1600 °C.

3.2 Analysis of XRD and EDX on the New Phase BZY424

To investigate the phase relationship of the BaO-ZrO₂-YO₁.₅ system around the composition of new phase (BZY424 phase), we made samples whose composition is near to the new phase. The compositions of quenched samples were $X_{BaO} = 0.411$, $X_{ZrO_2} = 0.166$, and $X_{YO_{1.5}} = 0.421$ (sample H), and $X_{BaO} = 0.421$, $X_{ZrO_2} = 0.196$, and $X_{YO_{1.5}} = 0.381$ (sample I).

The compositions of grains in the samples analyzed by EDX are shown on pseudoternary phase diagrams of the BaO-ZrO₂-YO₁.₅ system in Fig. 4(c) and (d), and summarized in Table 2. In both samples, grains with composition near to BZY424 phase were observed, but the samples were not in a single phase region. In addition, BaO-rich grains were observed in Fig. 4(c) and (d) and Table 2, according to Kojima et al.[23] these grains should be solidified liquid phase. As seen in Table 2, four types of grains existed in sample I, which does not obey the phase rule. Some kinds of grains might be decomposition products from liquid phase during cooling.

XRD patterns of samples H and I are shown in Fig. 6, and the identified phases are summarized in Table 1. In samples H and I, there were clear peak patterns of yttria phase. Considering the existence of liquid phase in both samples H and I and experimental results of the Section 3.1,
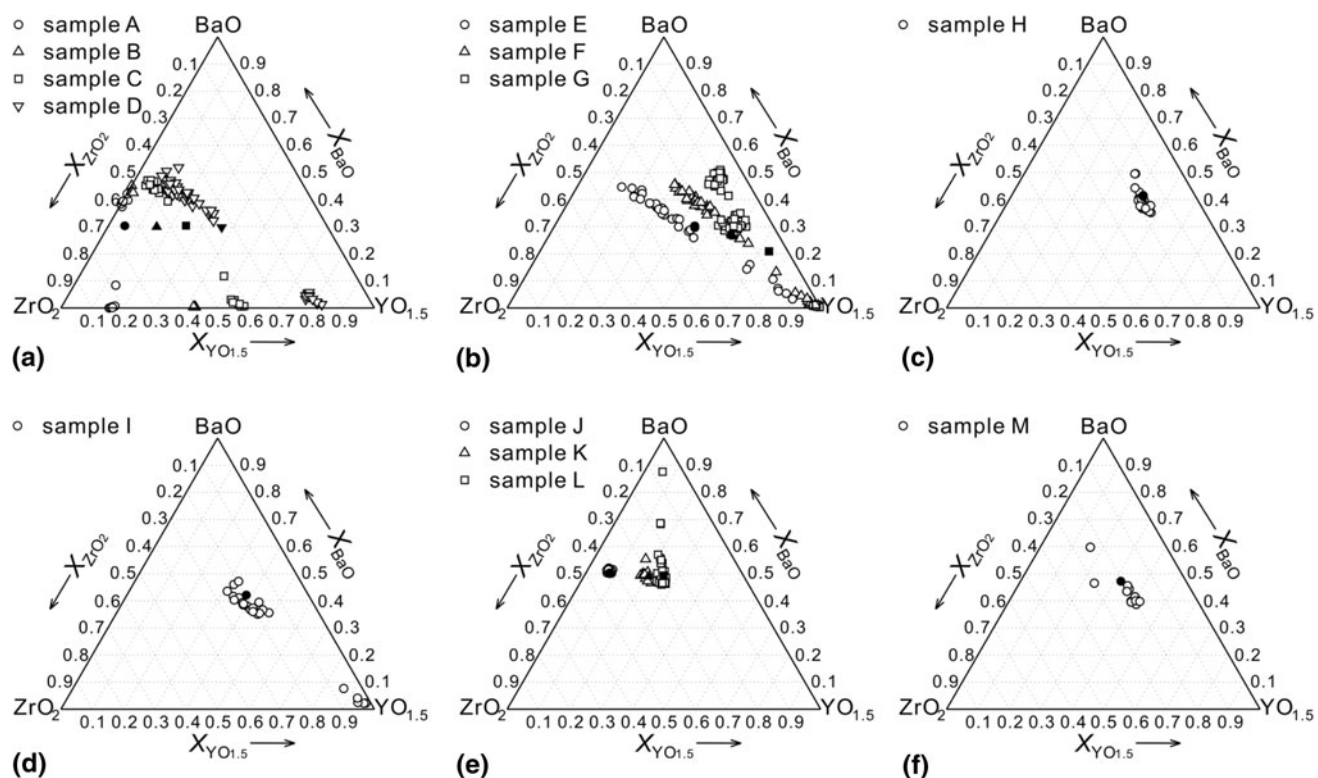
Fig. 4 Results of EDX analysis in samples after heat-treatment at 1600 °C for 24 h on pseudoternary phase diagrams of the BaO-ZrO$_2$-YO$_{1.5}$ system ((a) samples A to D, (b) samples E to G, (c) sample H, (d) sample I, (e) samples J to L, (f) sample M). Filled point is an average composition of each sample

Table 2 Compositions of each grain in samples after heat-treatment at 1600 °C for 24 h by EDX analysis

Sample	Barium zirconate (Perovskite)			New phase (Perovskite)			ZrO$_2$			Y$_2$O$_3$			Trace of liquid phase		
	X_{BaO}	X_{ZrO_2}	$X_{YO_{1.5}}$	X_{BaO}	X_{ZrO_2}	$X_{YO_{1.5}}$	X_{BaO}	X_{ZrO_2}	$X_{YO_{1.5}}$	X_{BaO}	X_{ZrO_2}	$X_{YO_{1.5}}$	X_{BaO}	X_{ZrO_2}	$X_{YO_{1.5}}$
A	0.42	0.58	0.00		(n.d.)		0.00	0.85	0.15		(n.d.)			(n.d.)	
B	0.43	0.56	0.01		(n.d.)		0.00	0.57	0.43		(n.d.)			(n.d.)	
C	0.49	0.47	0.04		(n.d.)		0.00	0.42	0.58		(n.d.)			(n.d.)	
D	0.49	0.44	0.07		(n.d.)			(n.d.)		0.01	0.16	0.83		(n.d.)	
E	0.45	0.41	0.14		(n.d.)			(n.d.)		0.03	0.07	0.89		(n.d.)	
F	0.46	0.24	0.31	0.38	0.20	0.43		(n.d.)		0.01	0.00	0.99		(n.d.)	
G		(n.d.)		0.31	0.16	0.53		(n.d.)		0.01	0.00	0.99	0.47	0.12	0.41
H		(n.d.)		0.36	0.18	0.47		(n.d.)			(n.d.)		0.50	0.15	0.35
I	0.44	0.25	0.31	0.35	0.17	0.48		(n.d.)		0.02	0.02	0.96	0.46	0.22	0.32
J	0.50	0.42	0.08		(n.d.)			(n.d.)			(n.d.)			(n.d.)	
K	0.47	0.31	0.23		(n.d.)			(n.d.)			(n.d.)			(n.d.)	
L	0.46	0.28	0.26		(n.d.)			(n.d.)			(n.d.)		0.69	0.17	0.15
M	0.47	0.30	0.24	0.40	0.19	0.42		(n.d.)			(n.d.)		0.60	0.24	0.16

yttria phase might be the decomposition product from liquid phase. In sample H, combining the results of EDX analysis, the peaks other than those of yttria should come from BZY424 phase in sample H. Compared with the XRD patterns of samples H and I, two peaks around 30 degrees are barely visible in sample I. This is because peaks of cubic barium zirconate phase (BaZrO$_3$(ss)) overlapped to peaks of BZY424 phase. Thus, it is considered that sample I consists

of BZY424 phase and cubic barium zirconate phase (BaZrO$_3$(ss)) with very small amount of Y$_2$O$_3$ phase.

3.3 Analysis of X-ray Diffraction and Results of EDX Analysis of Samples of X_{BaO} = 0.50 at 1600 °C

Samples on the composition line of X_{BaO} = 0.50 (samples J to M) were prepared in order to confirm the solubility
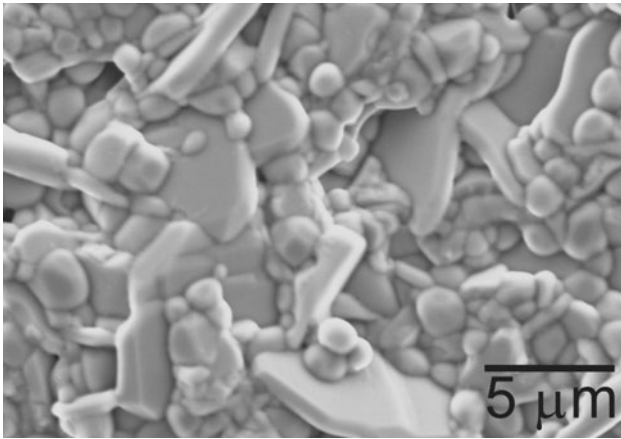
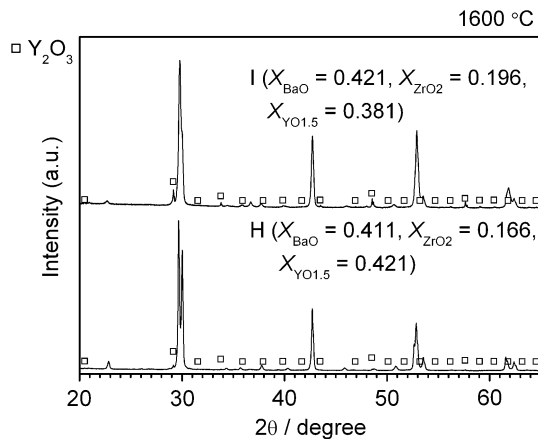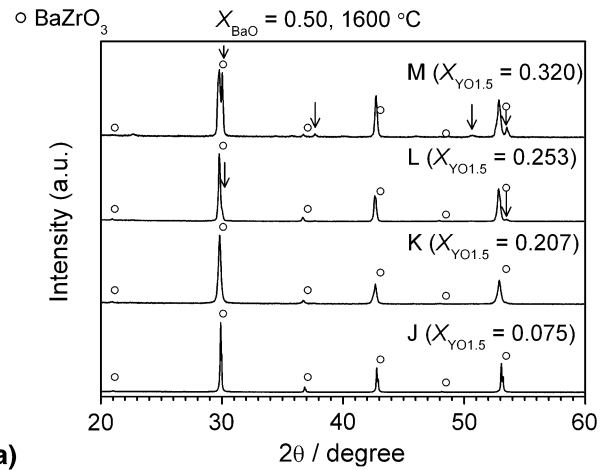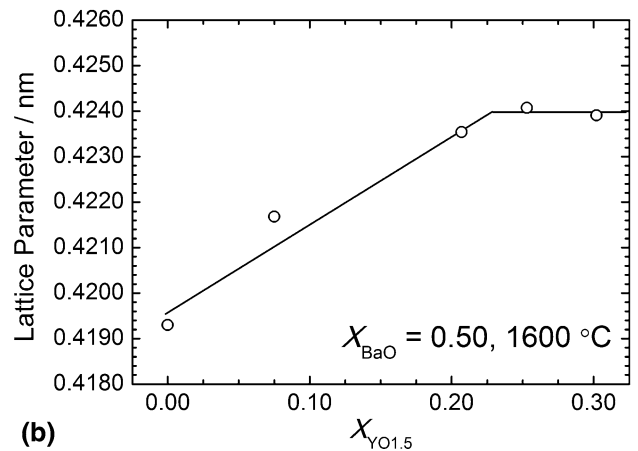**Fig. 5** SEM images of sample G after heat-treatment at 1600 °C

Fig. 6 XRD patterns of samples H and I after heat-treatment at 1600 °C for 24 h. Each symbol indicates diffraction patterns of □ (Y_2O_3, JCPDS No. 00-043-1036)

Fig. 7 (a) XRD patterns of samples at $X_{BaO} = 0.50$ after heat-treatment at 1600 °C for 24 h. Each symbol indicates diffraction patterns of ○ ($BaZrO_3$, JCPDS No. 00-006-0399). Unknown peaks are indicated by *arrows*, ↓. (b) Lattice parameters of barium zirconate phase as a function of the mole fraction of yttria, $X_{YO_{1.5}}$

of yttria into barium zirconate. Figure 7(a) shows XRD patterns of samples at $X_{BaO} = 0.50$ which were heat-treated at 1600 °C for 24 h, and the identified phases are summarized in Table 1. In sample J ($X_{YO_{1.5}} = 0.075$), only the cubic barium zirconate phase ($BaZrO_3$(ss)) was detected, and this was also confirmed by EDX analysis as shown in Fig. 4(e). In sample K ($X_{YO_{1.5}} = 0.207$), only the cubic barium zirconate phase ($BaZrO_3$(ss)) was detected, but a grain with BaO-rich composition was observed by EDX analysis as shown in Fig. 4(e). The grain is considered to be a trace of liquid phase. In sample L ($X_{YO_{1.5}} = 0.253$) and M ($X_{YO_{1.5}} = 0.320$), peak patterns similar to BZY424 phase are shown by arrows were identified in addition to those of cubic barium zirconate phase ($BaZrO_3$(ss)). From the result of EDX analysis in Table 2, one of the detected phases in sample M ($X_{BaO} = 0.40$, $X_{ZrO_2} = 0.19$, and $X_{YO_{1.5}} = 0.42$) corresponds indeed to BZY424 phase. Although BZY424 phase was not detected in sample L by EDX analysis, the unknown phase of sample L detected by XRD should be

BZY424 phase. Combining the results of EDX analysis in samples F, G, H, I, and M, BZY424 phase forms wide solid solution. The composition of BZY424 seems to be from 0.31 to 0.40 in X_{BaO}, from 0.16 to 0.20 in X_{ZrO_2} and from 0.42 to 0.53 in $X_{YO_{1.5}}$. Figure 7(b) shows the variation of lattice parameters of cubic barium zirconate phase ($BaZrO_3$(ss)) in samples J to M as a function of the mole fraction of yttria, $X_{YO_{1.5}}$ together with the lattice parameter of non-doped barium zirconate ($X_{YO_{1.5}} = 0$) [JCPDS card No. 00-006-0399, lattice parameter, $a = 0.419300$ nm]. Lattice parameters of cubic barium zirconate phase ($BaZrO_3$(ss)) increased by doping yttrium until between $X_{YO_{1.5}} = 0.207$ and 0.253. This is because the ionic radius of an yttrium ion (Y^{3+}: 0.0900 nm[37]), which is doped into zirconium sites, is larger than that of a zirconium ion (Zr^{4+}: 0.072 nm[37]). However, the lattice parameter is almost constant at higher compositions of yttria, which locate in two or three phase regions. This indicates that the solubility of yttria into cubic barium zirconate at $X_{BaO} = 0.50$ is

between $X_{YO_{1.5}} = 0.207$ and 0.253. Even by EDX analysis, the mole fraction of yttria in the cubic barium zirconate phase of samples L and M were 0.24 and 0.26, respectively. Thus, the solubility of yttria into barium zirconate is determined to be $X_{YO_{1.5}} = 0.25$ at 1600 °C. Therefore, we confirmed that there is no phase separation at the composition of 15% yttrium-doped barium zirconate at 1600 °C. Also, in samples K, L, and M, the cubic barium zirconate phase (BaZrO$_3$(ss)) had barium deficiency as shown

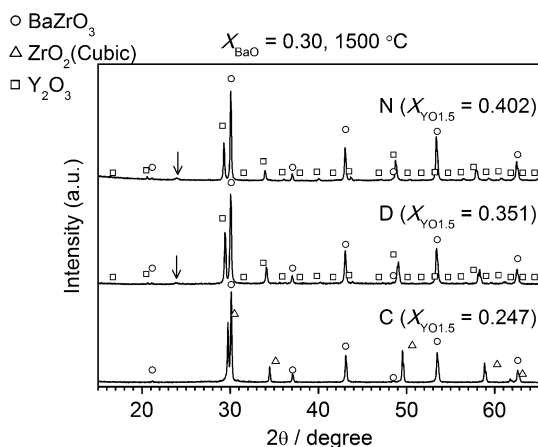**Fig. 8** XRD patterns of samples at $X_{BaO} = 0.30$ after heat-treatment at 1500 °C for 100 h ($X_{YO_{1.5}} = 0.247$, 0.351 and 0.402). Each symbol indicates diffraction patterns of ○ (BaZrO$_3$, JCPDS No. 00-006-0399), △ (ZrO$_2$, JCPDS No. 00-027-0997), □ (Y$_2$O$_3$, JCPDS No. 00-043-1036). Unknown peaks are indicated by *arrows*, ↓

in Table 2. This might in part be because of yttrium ion occupancy of barium sites.

3.4 Phase Relationship of the BaO-ZrO$_2$-YO$_{1.5}$ System at 1500 °C

It was reported by Oyama et al. that another barium zirconate phase, whose composition is $X_{BaO} = 0.50$, $X_{ZrO_2} = 0.33$, and $X_{YO_{1.5}} = 0.17$, exists at 1600 °C. They called it BZ(II) phase.[23,38] We could not find the existence of BZ(II) phase at 1600 °C, but considered that BZ(II) phase was one of the compounds which are formed by the phase separation of 15% yttrium-doped barium zirconate at synthesizing temperature, 1300 °C. We therefore examined samples to confirm the existence of the reported barium zirconate phase at temperatures lower than 1600 °C. Samples on the composition line of $X_{BaO} = 0.30$ (samples C, D, and N) were heat-treated at 1500 °C for 100 h in air. XRD patterns of these samples are shown in Fig. 8 and compositions of grains analyzed by EDX are shown on the plots of the pseudoternary phase diagram of the BaO-ZrO$_2$-YO$_{1.5}$ system in Fig. 9. The composition of each grain was summarized in Table 3. At $X_{YO_{1.5}} = 0.247$ (sample C), cubic barium zirconate phase (BaZrO$_3$(ss)) and cubic zirconia phase were identified and the results measured by EDX also support that by XRD. When $X_{YO_{1.5}} = 0.351$ (sample D), cubic barium zirconate phase (BaZrO$_3$(ss)), yttria phase and one unknown peak were identified by XRD. Although peak patterns of yttria phase is similar to that of cubic zirconia phase, we judged that the yttria phase was detected in sample D because minor peaks of yttria phase were identified at the angles of 20.7, 36.2, 40.2, 43.9, 56.7, 59.6° as shown in Fig. 8. But, only cubic barium zirconate
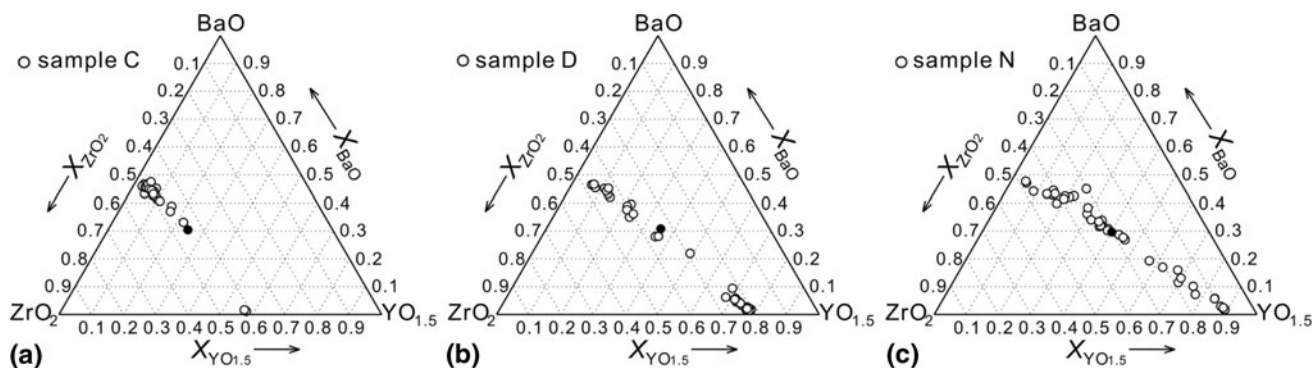

Fig. 9 Results of EDX analysis in samples after heat-treatment at 1500 °C for 100 h on pseudoternary phase diagrams of the BaO-ZrO$_2$-YO$_{1.5}$ system ((a) sample C, (b) sample D, (c) sample N). Filled point is an average composition of each sample

Table 3 Compositions of each grain in samples after heat-treatment at 1500 °C for 100 h by EDX analysis

	Barium zirconate (Perovskite)			ZrO$_2$			Y$_2$O$_3$			Unknown phase		
	X_{BaO}	X_{ZrO_2}	$X_{YO_{1.5}}$	X_{BaO}	X_{ZrO_2}	$X_{YO_{1.5}}$	X_{BaO}	X_{ZrO_2}	$X_{YO_{1.5}}$	X_{BaO}	X_{ZrO_2}	$X_{YO_{1.5}}$
C	0.47	0.50	0.03	0.01	0.41	0.58		(n.d.)			(n.d.)	
D	0.46	0.47	0.06		(n.d.)		0.02	0.21	0.77		(n.d.)	
N	0.45	0.51	0.03		(n.d.)		0.02	0.09	0.89	0.45	0.30	0.25

phase (BaZrO$_3$(ss)) and yttria phase was detected by EDX analysis as shown in Fig. 9(b) and Table 3. At $X_{YO_{1.5}} = 0.402$ (sample N), cubic barium zirconate phase (BaZrO$_3$(ss)), yttria phase and one unknown peak were also identified by XRD. We judged that yttria phase was detected in sample N for the same reason as sample D. In addition to yttria phase, there were two kinds of grains of barium zirconate phase as shown in Fig. 9(a) and Table 3. A grain with $X_{BaO} = 0.45$, $X_{ZrO_2} = 0.30$, and $X_{YO_{1.5}} = 0.25$ might be a mixture of large amount of BZ(II) phase and small amount of yttria phase. The unknown peak detected by XRD in sample N and D might relate to diffraction from BZ(II) phase. A possibility for the existence of BZ(II) is suggested in this study, but further investigation is necessary in order to clarify.

4. Conclusions

A part of a pseudoternary phase diagram in a BaO-ZrO$_2$-YO$_{1.5}$ system at 1600 °C was established, and we confirmed that there is no phase separation at the composition of 15% yttrium-doped barium zirconate at 1600 °C. According to the phase diagram, we found the new phase, BZY424 phase, with the composition range from 0.31 to 0.40 in X_{BaO}, from 0.16 to 0.20 in X_{ZrO_2} and from 0.42 to 0.53 in $X_{YO_{1.5}}$. Diffraction patterns of BZY424 phase is similar to cubic barium zirconate phase (BaZrO$_3$(ss)). Additionally, we determined that the solubility of yttria into cubic barium zirconate was $X_{YO_{1.5}} = 0.25$ at 1600 °C. There might be another new phase at 1500 °C, whose composition is close to the previously reported BZ(II) phase.

References

1. K.D. Kreuer, Aspects of the Formation and Mobility of Protonic Charge Carriers and the Stability of Perovskite-type Oxides, *Solid State Ionics*, 1999, **125**, p 285-302
2. H.G. Bohn and T. Schober, Electrical Conductivity of the High-Temperature Proton Conductor BaZr$_{0.9}$Y$_{0.1}$O$_{2.95}$, *J. Am. Ceram. Soc.*, 2000, **83**, p 768-772
3. T. Schober and H.G. Bohn, Water Vapor Solubility and Electrochemical Characterization of the High Temperature Proton Conductor BaZr$_{0.9}$Y$_{0.1}$O$_{2.95}$, *Solid State Ionics*, 2000, **127**, p 351-360
4. K.D. Kreuer, S. Adams, W. Munch, A. Fuchs, U. Klock, and J. Maier, Proton Conducting Alkaline Earth Zirconates and Titanates for High Drain Electrochemical Applications, *Solid State Ionics*, 2001, **145**, p 295-306
5. K.D. Kreuer, Proton-Conducting Oxides, *Annu. Rev. Mater. Res.*, 2003, **33**, p 333-359
6. W.S. Wang and A.V. Virkar, Ionic and Electron-Hole Conduction in BaZr$_{0.93}$Y$_{0.07}$O$_{3-\delta}$ by 4-probe DC Measurements, *J. Power Sources*, 2005, **142**, p 1-9
7. F. Iguchi, T. Yamada, N. Sata, T. Tsurui, and H. Yugami, The Influence of Grain Structures on the Electrical Conductivity of a BaZr$_{0.95}$Y$_{0.05}$O$_3$ Proton Conductor, *Solid State Ionics*, 2006, **177**, p 2381-2384
8. S. Tao and J.T.S. Irvine, Conductivity Studies of Dense Yttrium-doped BaZrO$_3$ Sintered at 1325 °C, *Solid State Chem.*, 2007, **180**, p 3493-3503
9. K. Nomura and H. Kageyama, Transport Properties of Ba(Zr$_{0.8}$Y$_{0.2}$)O$_{3-\delta}$ Perovskite, *Solid State Ionics*, 2007, **178**, p 661-665
10. P. Babilo, T. Uda, and S.M. Haile, Processing of Yttrium-Doped Barium Zirconate for High Proton Conductivity, *J. Mater. Res.*, 2007, **22**, p 1322-1330
11. S.B.C. Duval, P. Holtappels, U.F. Vogt, E. Pomjakushina, K. Conder, U. Stimming, and T. Graule, Electrical Conductivity of the Proton Conductor BaZr$_{0.9}$Y$_{0.1}$O$_{3-\delta}$ Obtained by High Temperature Annealing, *Solid State Ionics*, 2007, **178**, p 1437-1441
12. F. Iguchi, N. Sata, T. Tsurui, and H. Yugami, Microstructures and Grain Boundary Conductivity of BaZr$_{1-x}$Y$_x$O$_3$ (x = 0.05, 0.10, 0.15) Ceramics, *Solid State Ionics*, 2007, **178**, p 691-695
13. J.M. Serra and W.A. Meulenberg, Thin-Film Proton BaZr$_{0.85}$Y$_{0.15}$O$_3$ Conducting Electrolytes: Toward an Intermediate-Temperature Solid Oxide Fuel Cell Alternative, *J. Am. Ceram. Soc.*, 2007, **90**(7), p 2082-2089
14. A.K. Azad, C. Savaniu, S. Tao, S. Duval, P. Holtappels, R.M. Ibberson, and J.T.S. Irvine, Structural Origins of the Differing Grain Conductivity Values in BaZr$_{0.9}$Y$_{0.1}$O$_{2.95}$ and Indication of Novel Approach to Counter Defect Association, *J. Mater. Chem.*, 2008, **18**, p 3414-3418
15. N. Ito, H. Matsumoto, Y. Kawasaki, S. Okada, and T. Ishihara, Introduction of In or Ga as Second Dopant to BaZr$_{0.9}$Y$_{0.1}$O$_{3-\delta}$ to Achieve Better Sinterability, *Solid State Ionics*, 2008, **179**, p 324-329
16. A. D'Epifanio, E. Fabbri, E. DiBartolomeo, S. Licoccia, and E. Traversa, Design of BaZr$_{0.8}$Y$_{0.2}$O$_{3-\delta}$ Protonic Conductor to Improve the Electrochemical Performance in Intermediate Temperature Solid Oxide Fuel Cells (IT-SOFCs), *Fuel Cells*, 2008, **8**, p 69-76
17. S. Higgins, N.M. Sammes, A. Smirnova, J.A. Kikner, and G. Tompsett, Yttrium-Doped Barium Zirconates as Ceramic Conductors in the Intermediate Temperature Range, *J. Fuel Cell Sci. Technol.*, 2008, **5**, p 011003
18. S. Imashuku, T. Uda, Y. Nose, G. Taniguchi, Y. Ito, and Y. Awakura, Dependence of Dopant Cations on Microstructure and Proton Conductivity of Barium Zirconate, *J. Electrochem. Soc.*, 2009, **156**(1), p B1-B8
19. S. Imashuku, T. Uda, and Y. Awakura, Sintering Properties of Trivalent Cation-Doped Barium Zirconate at 1600 °C, *Electrochem. Solid-State Lett.*, 2007, **10**(10), p B175-B178
20. S. Imashuku, T. Uda, Y. Nose, K. Kishida, S. Harada, H. Inui, and Y. Awakura, Improvement of Grain-Boundary Conductivity of Trivalent Cation-Doped Barium Zirconate Sintered at 1600 °C by Co-doping Scandium and Yttrium, *J. Electrochem. Soc.*, 2008, **155**(6), p B581-B586

21. S. Imashuku, T. Uda, Y. Nose, Y. Ito, and Y. Awakura, Effect of Isovalent Cation Substitution on Conductivity and Microstructure of Sintered Yttrium-Doped Barium Zirconate, *J. Alloy. Compd.*, 2010, **409**, p 672-676

22. S. Imashuku, T. Uda, Y. Nose, and Y. Awakura, Fabrication and Electrical Characterization of 15% Yttrium-doped Barium Zirconate – Nitrate Freeze Drying Method Combined with Vacuum Heating, *J. Electrochem. Soc.*, submitted

23. A. Kojima, K. Tanaka, Y. Oyama, T. Higuchi, and S. Yamaguchi, Phase Equilibrium and Thermodynamic Stability in the BaO-ZrO$_2$-YO$_{1.5}$ System, *The 31st Symposium on Solid State Ionics in Japan*, 2005, p 100-101

24. I. Barin, *Thermochemical Data of Pure Substances*, 3rd ed., VCH Verlagsgesellschaft mbH, Tokyo, 1995

25. J.O.A. Paschoal, H. Kleykamp, and F. Thümmler, Phase Equilibria in the Pseudoquaternary BaO-UO$_2$-ZrO$_2$-MoO$_2$ System, *J. Nucl. Mater.*, 1987, **151**, p 10-21

26. R.S. Roth, *Proceedings of User Aspects of Phase Equilibria*, Petten, 1990, p 153-168

27. J. Sestak, J. Kamarad, P. Holba, A. Triska, E. Pollert, and M. Nevriva, Charge-Distribution, Pressure and Composition Effects of CuO$_x$ Based Superconductors, *Thermochim. Acta*, 1991, **174**, p 99-114

28. W. Zhang and K. Osamura, Phase-Equilibrium in Y-Ba-O System, *Mater. Trans.*, 1991, **32**(11), p 1048-1052

29. I. Horsak, J. Sestak, and B. Stepanek, Simple Computer-Program Used for the Calculation of Stable and Metastable Phase-Boundary Lines for the Pseudobinary Edges in the BaO-CuO$_x$-YO$_{1.5}$ System, *Thermochim. Acta*, 1994, **234**, p 233-243

30. K.K. Srivastava, R.N. Patil, C.B. Choudhary, K.V.G.K. Gokhale, and E.C. Subbarao, Revised Phase-Diagram of System ZrO$_2$-YO$_{1.5}$, *Trans. J. Br. Ceram. Soc.*, 1974, **73**(5), p 85-91

31. V.S. Stubican, Phase Equilibria and Metastability in Some Zirconia Systems, *Science and Technology of Zirconia III*, S. Somiya, N. Yamamoto, and H. Yanagida, Ed., Sept 9-10, 1986, American Ceramic Society, Tokyo, 1988, p 71-82

32. F.K. Fan, A.K. Kuznetsov, and E.K. Keler, *Bull. Acad. Sci. USSR Div. Chem. Sci.*, 1963, **4**, p 542-549

33. A. Rouanet, Contribution to Study of Zirconium-Oxides Systems of Lanthanides Close to Melting Point, *Rev. Int. Ht.-Temp. Refract.*, 1971, **8**(2), p 161-180

34. H.G. Scott, Phase Relationship in Zirconia-Yttria System, *J. Mater. Sci.*, 1975, **10**(9), p 1527-1535

35. C. Pascual and P. Duran, Subsolidus Phase-Equilibria and Ordering in the System ZrO$_2$-Y$_2$O$_3$, *J. Am. Ceram. Soc.*, 1983, **66**, p 23-27

36. M. Yashima, M. Kakihana, and M. Yoshimura, Metastable-Stable Phase Diagrams in the Zirconia-Containing Systems Utilized in Solid-Oxide Fuel Cell Application, *Solid State Ionics*, 1996, **86-88**, p 1131-1149

37. R.D. Shannon, Revised Effective Ionic-radii and Systematic Studies of Interatomic Distances in Halides and Chalcogenides, *Acta Crystallogr. A: Cryst. Phys. Diffr. Theor. Gen. Crystallogr.*, 1976, **32**, p 751-767

38. Y. Oyama, X. Li, S. Miyoshi, and S. Yamaguchi, Stability and Transformation of Ba$_3$Zr$_2$O$_{8.5}$ Phase, *Proceedings of the 14th International Conference on Solid State Protonic Conductors*, Sept 7-11, 2008 (Kyoto), p 120